The black hole fundamental plane from a uniform sample of radio and X-ray emitting broad line AGNs

Ran Wang and Xue-Bing Wu

Astronomy Department, Peking University, Beijing 100871, China

littlestar@pku.edu.cn; wuxb@bac.pku.edu.cn

Min-Zhi Kong

National Astronomical Observatories, Chinese Academy of Sciences, Beijing 100012, China

kmz@bao.ac.cn

ABSTRACT

We derived the black hole fundamental plane relationship among the 1.4GHz radio luminosity (L_r), 0.1-2.4keV X-ray luminosity (L_X), and black hole mass (M) from a uniform broad line SDSS AGN sample including both radio loud and radio quiet X-ray emitting sources. We found in our sample that the fundamental plane relation has a very weak dependence on the black hole mass, and a tight correlation also exists between the Eddington luminosity scaled X-ray and radio luminosities for the radio quiet subsample. Additionally, we noticed that the radio quiet and radio loud AGNs have different power-law slopes in the radio–X-ray non-linear relationship. The radio loud sample displays a slope of 1.39, which seems consistent with the jet dominated X-ray model. However, it may also be partly due to the relativistic beaming effect. For radio quiet sample the slope of the radio–X-ray relationship is about 0.85, which is possibly consistent with the theoretical prediction from the accretion flow dominated X-ray model. We briefly discuss the reason why our derived relationship is different from some previous works and expect the future spectral studies in radio and X-ray bands on individual sources in our sample to confirm our result.

Subject headings: accretion, accretion disks — galaxies: active — galaxies: nuclei — radio continuum: galaxies — X-ray: galaxies

1. Introduction

In black hole systems, the central black hole accretion process is believed to be the dominated energy producing mechanism, sometimes also accompanied with a relativistic jet. Observationally, such kinds of disk-jet systems display similar characteristics of strong X-ray and radio emissions, and exist at different scales from the stellar mass black hole X-ray binaries (XRBs) to active galactic nuclei (AGNs). Recently the non-linear relationship among the central X-ray emission, core radio emission and black hole mass, also called as the black hole fundamental plane, has been investigated in details both theoretically and observationally (eg. Merloni et al. 2003, Heinz & Sunyaev 2003, Falcke et al. 2004). This relationship may directly reflect the common physics of a disk-jet system around the black hole.

The radio–X-ray correlation has been widely studied in the Galactic black hole candidates (Fender et al. 2003; Gallo et al. 2003; Yuan & Cui 2005) and has been also extended to AGNs (Merloni et al. 2003; Falcke et al. 2004). Gallo et al. (2003) investigated a sample of ten low/hard state Galaxy black hole X-ray binaries and found that all sources in the low/hard state follow a universal power-law relation between the radio and X-ray emissions with a slope of 0.7 (i.e. $L_R \propto L_X^{0.7}$). Additionally, they suggested that when the system enters the hard to soft transition state the jet is suppressed and the radio emission drops. Merloni et al. (2003) collected a large sample containing both Galactic black hole X-ray binaries and AGNs, and gave a fundamental plane relation among the radio luminosity ($L_{R\,(5GHz)}$), X-ray luminosity ($L_{X\,(2-10keV)}$) and black hole mass (M_{BH}). Their result can be expressed as $L_{R\,(5GHz)} \propto L^{0.6}_{X\,(2-10keV)} M^{0.78}_{BH}$ and the power-law slope of the radio–X-ray relation is consistent with that previously obtained for stellar black hole systems (Gallo et al. 2003).

Physics explanations on the derived radio–X ray correlation have been also widely discussed. The radio emission is always believed to be the synchrotron radiation from the jet while the X-ray emission can come from both the accretion flow and the relativistic jet in a disk-jet system. At high accretion rate the X-ray emission is mainly from accretion flow and its dependence on black hole mass and accretion rate can be different according to different accretion disk model (Shakura & Sunyaev 1973; Narayan & Yi 1994; Merloni & Fabian 2002). Merloni et al. (2003) has investigated the cases of several different disk models and found a good agreement between their fitting result and the radiation inefficient accretion flow models. When the accretion rate drops, the X-ray emission declines according to these models. Below a certain critical value ($L/L_{Edd} \sim 10^{-5} - 10^{-6}$, where L_{Edd} is the Eddington luminosity), the jet emission will become dominant (Gallo et al. 2003; Yuan & Cui 2005). In such a 'low' state where jet dominates the X-ray emission, the power-law slope of

the radio–X-ray relation should be greater than 1 (Heinz 2004; Yuan & Cui 2005). This means that when the X-ray emission is dominated by jet, the slope of the fundamental plane relation is probably different from the case when the X-ray emission is dominated by the accretion flow.

However, the reliability of the fundamental plane relation given by Merloni et al. (2003) has been questioned. Recently Bregman (2005) pointed out that the fundamental plane relation in Merloni et al. (2003) can be led out even with those sources having only upper limit of radio emission or by scrambling the radio fluxes and making them randomly assigned to the sources in the whole sample. In addition, the sample in Merloni et al. (2003) has the ratios of X-ray luminosity to Eddington luminosity in a large range, from lower than 10^{-6} to 1. So the X-ray luminosity may have different dominated mechanisms according to different level of luminosities and thus has different dependences on the accretion rate according to the accretion disk models. This may cause significant scatters of the intrinsic black hole fundamental plane relation. Furthermore, the sample in Merloni et al. (2003) consists of both Galactic and extragalactic sources with estimated black hole mass and is therefore not uniform. Various selection effects may also seriously affect the derived black hole fundamental plan relation.

In this paper we select a uniform sample of broad line AGNs based on the cross-identifications of ROSAT all-sky survey, Sloan Digital Sky Survey and FIRST 20cm radio survey. With this sample we can possibly avoid the bias from both the inhomogeneous source selections and the data quality differences, and then better study the black hole fundamental plane relation for broad line AGNs. The sample selection and data reduction process are described in section 2 and statistical results are given in section 3. The possible theoretical explanations are discussed in section 4.

Through out this paper, we adopt the cosmology model with $H_0 = 70\,kms^{-1}Mpc^{-1}$, $\Omega_\Lambda = 0.7$, and $\Omega_M = 0.3$.

2. The Sample

2.1. Sample selection

Our sample is selected from the X-ray emitting SDSS AGN catalog (Anderson et al. 2003) and the FIRST 20 cm radio survey (White et al. 1997; Becker et al. 2003). The AGN catalog of Anderson et al. (2003) was selected based on the cross-identifications of the ROSAT all-sky survey (RASS) and the Sloan Digital Sky Survey (SDSS). As discussed by Anderson et al. (2003), the RASS and SDSS are extremely well-matched both in the detection

area and sensitivity. With the additional information from the FIRST radio observations, about 10^4 RASS X-ray sources are searched for the SDSS optical counterparts. As an initial and important result, Anderson et al. (2003) obtained a uniform sample of more than 1200 X-ray emitting quasars and other AGNs over the 1400 deg^2 of the sky, including 964 broad permitted line AGNs (FWHM>1000km/s), 216 narrow permitted line AGNs (FWHM<1000km/s) and 45 BL Lac candidates.

One of the benefits of this sample, as Anderson et al. (2003) pointed out, is that the RASS and SDSS survey area is also covered by the FIRST 20cm radio survey. So we select all the FIRST radio detected sources in the broad line AGN catalog and finally construct a ROSAT-SDSS-FIRST cross-identified sample of 132 broad permitted line AGNs. All of these 132 sources have 0.1 - 2.4keV X-ray measurement from RASS and 1.4GHz radio measurement from the FIRST 20cm survey. The optical spectra of these sources are available from the SDSS data archive, which can be used to estimate the central black hole masses of them. For this purpose we analyze the SDSS spectra and the data reduction process is described in the following section.

2.2. Data reduction and black hole mass estimation

We examined all of the 132 spectra first with an aim that we can finally estimate the black hole mass of AGNs with broad permitted lines (eg. $H\beta\lambda4861, MgII\lambda2798$). We excluded the spectra in poor quality (with no visible emission lines) or with no Hβ or MgII λ2798 lines in the observation wavelength. At last we get the final sample of 115 objects with black hole mass estimatable from either Hβ λ4861 or MgII λ2798 broad emission line (Kaspi et al. 2000; McLure & Jarvis 2002; Wu et al. 2004). One thing should be mentioned is that there are four high redshift ($z > 2$) sources with only the CIV λ1549 broad emission line available for black hole mass estimation in their SDSS spectra. Because we want to reduce the scatters in black hole mass introduced by different mass estimation methods and the number of these high redshift sources is rather small, we exclude these four source in our analysis as well.

We made the corrections for the Galactic extinction and redshift effects and subtracted the iron emission from the continuum. The UV and optical iron templates were adopted from Vestergaard & Wikes (2001) and Boroson & Green (1992) in the wavelength range $1250\mathring{A} < \lambda_{rest} < 3100\mathring{A}$ and $4250\mathring{A} < \lambda_{rest} < 7000\mathring{A}$, respectively.

Then we fit the continuum and emission lines with the *Mpfit* package in IDL [1], which was developed based on the Levenberg-Marquardt technique. The continuum fitting process was performed in the two Iron template windows respectively. Then we fit each band of the continuum with a power-law and calculate the rest-frame continuum flux density at 3000$\mathring{A}$, and 4400$\mathring{A}$. For high redshift sources, the rest-frame optical band moves out of the SDSS window and the 4400$\mathring{A}$ flux density cannot be fitted directly. So we extrapolate the power law fitting in the UV band to the optical band and calculate the 4400$\mathring{A}$ flux density for these sources. Finally we fit the emission lines with the gaussian profiles. We apply one gaussian component for MgII λ2798 line and two gaussians for the broad and narrow components for Hβ λ4861. From the fittings we can get the values of flux and FWHM of these emission lines.

The 3000$\mathring{A}$, 4400$\mathring{A}$, and Hβ luminosities, as well as the 0.1-2.4keV X-ray luminosity with data from RASS and rest frame 1.4GHz radio luminosity with data from FIRST, are calculated for these 115 AGNs. We also derive their rest-frame 5GHz flux from the 1.4GHz data by assuming a power-law index of 0.5 (i.e. $f_\nu \propto \nu^{-0.5}$). Then the radio loudness is derived with the rest frame 4400$\mathring{A}$ and 5GHz flux density according to the definition $R = f_{5GHz}/f_b$ (Kellermann et al. 1989). The radio loud and radio quiet sources are divided by $R = 10$. Our sample consists of 39 radio quiet sources and 76 radio loud sources.

Finally, the black hole masses for all of these 115 sources are estimated. For the broad line AGNs, the black hole mass can be estimated with the velocity and radius of the broad line region (BLR) using the formula in Kaspi et al. (2000),

$$M = 1.464 \times 10^5 (\frac{R_{BLR}}{light - days})(\frac{V_{FWHM}}{10^3 kms^{-1}})^2 M_\odot, \quad (1)$$

where V_{FWHM} is the full width at half maximum (FWHM) of the broad emission lines and R_{BLR} is the radius of the broad line region.

For the sources with Hβ λ4861 line measured, V_{FWHM} is the FWHM of the broad component of Hβ emission line and R_{BLR} can be determined using the broad Hβ line luminosity ($L_{H\beta}$) with the empirical relation provided by Wu et al. (2004)(see also Kaspi et al. (2005)).

$$\mathrm{Log}R_{BLR}(light - days) = (1.381 \pm 0.080) + (0.684 \pm 0.106)\mathrm{Log}(L_{H\beta}/10^{42} ergs^{-1}). \quad (2)$$

For the sources with only MgII λ2798 line available, we adopt the empirical relation provided by McLure & Jarvis (2002):

$$M = 3.37(\frac{\lambda L_{3000}}{10^{44} ergs^{-1}})^{0.47}(\frac{V_{FWHM,MgII}}{kms^{-1}})^2 M_\odot, \quad (3)$$

[1]http://cow.physics.wisc.edu/ craigm/idl/idl.html

where λL_{3000} is the 3000$\mathring{A}$ continuum luminosity and $V_{FWHM,MgII}$ is the FWHM of the MgII emission line.

2.3. The sample properties

In this part we list some properties of our broad line AGN sample. Table 1 gives the total 115 sources with the SDSS optical source name, redshift, logarithm black hole mass in $M_\odot$, logarithm 0.1-2.4keV X-ray luminosity, logarithm rest frame 1.4GHz radio luminosity, and logarithm radio loudness in different columns. The sample include 39 radio quiet and 76 radio loud AGNs. In Fig. 1 we show the histograms of redshift, logarithm radio loudness (LogR), 0.1-2.4keV X-ray (L_X) and 1.4GHz radio (L_r) luminosities, black hole mass (M), and the logarithm ratio of X-ray to the Eddington luminosity. The redshift range for our sample is from 0.04 to nearly 2. The logarithm black hole masses distribute from about 6.7 to 9.7. Both the X-ray and radio luminosity distributions are in a broad range and cover more than 5 orders of magnitude. Additionally, the X-ray to Eddington luminosity ratio distributes from about $10^{-3.5}$ to 1.

In Fig. 2 we plot the radio luminosity against the X-ray luminosity with different symbols denoting different black hole mass bins. In the left panel we plot the logarithm luminosity while in the right panel we scale the luminosity with the Eddington luminosity. We do not see the clear trends that tracks of different mass bins are parallel to each other as that found in the former study (Merloni et al. 2003).

In Fig. 3 we re-plot the radio and X-ray luminosity, according to different radio loudness bins. We find that the sources obviously distributes in different parallel tracks according to different radio loudness.

3. Statistic results

In this section we present the correlation tests for the three fundamental plane variables, L_r, L_X, and M, and then give the fitting results.

3.1. Correlation tests

First of all, we perform the partial Kendall's τ test (Akritas & Siebert 1996) as did in Merloni et al. (2003) to test the intrinsic correlation among the three fundamental plane

parameters (i.e. M, L_X, and L_r), and in addition, among the Eddington luminosity scaled luminosities and black hole mass. Table 2 shows the results of this test, namely whether the correlation between X and Y is intrinsic or is only introduced by a third variable Z. The first three columns list the variables, the forth and fifth columns give the sub-sample type and number of object, and the last three columns list the partial Kendall's τ correlation coefficient, the square root of the calculated variance σ, and the probability to accept the null hypothesis. The null hypothesis will be rejected with a probability less than the significance level (i.e. ~ 0.05).

For the correlation between luminosities, the same dependence on the source distance always confuses the intrinsic physical relation. This is the main reason why the reality of the black hole fundamental plane relation is suspected (Bregman 2005). However, the partial correlation tests indeed prove that the luminosities are still strongly correlated even if the effect of distance is excluded. Furthermore, in order to avoid the distance effect we test the existence of the intrinsic relationship between radio and X-ray emissions by comparing the radio and X-ray fluxes of the AGNs in our sample. In Fig. 4 we plot the rest frame 1.4GHz radio flux versus the 0.1-2.4keV X-ray flux. We also plot the data of all the other sources (without FIRST detection) of the broad permitted line AGN sample in Table 2 of Anderson et al. (2003) as a comparison. For these sources we take 0.45mJy, the typical 3 σ detection level of the FIRST 20cm survey (White et al. 1997; Becker et al. 2003), as an upper limit of radio emission. We see that for these upper limit sources no correlations exist in the flux-flux plot, while for sources in our sample the radio and X-ray fluxes are clearly correlated in each radio loudness bins. For radio-quiet sources and radio-loud sources in 3 different radio-loudness bins, the Spearman correlation coefficients are 0.56, 0.27, 0.37 and 0.57 respectively. The corresponding power-law slope values for these different samples, derived from the Ordinary Least Square (OLS) bisector method (Isobe et al. 1990), are 0.60 ± 0.07, 1.10 ± 0.09, 1.05 ± 0.16 and 1.40 ± 0.30. Therefore, the intrinsic correlation between the radio and X-ray emissions of AGNs really exist, though the distance effect can stretch out the luminosity relationship significantly and affect the intrinsic relation seriously in a flux-limited AGN sample.

In addition, from Table 2 we can see that the correlations between the luminosities (L_r or L_X) and black hole masses still exist in the partial correlation test when taking the other luminosity (L_X or L_r) as the third variable. However, when considering the luminosities scaled with the Eddington luminosity, we see that for the radio quiet sample the correlation with the black hole mass disappears.

3.2. The black hole fundamental plane

Based on the correlation analysis above, we finally fit the data in the form of:

$$Log(\frac{L_r}{10^{40} erg\, s^{-1}}) = \xi_{RX} Log(\frac{L_X}{10^{44} erg\, s^{-1}}) + \xi_{RM} Log(\frac{M}{10^8 M_\odot}) + Const. \quad (4)$$

We also perform the fitting directly between the Eddington luminosity scaled radio and X-ray luminosities for the radio quiet sample in the form of:

$$Log(\frac{L_r}{L_{Edd}}) = \xi_{ERX} Log(\frac{L_X}{L_{Edd}}) + Const. \quad (5)$$

We apply the OLS multivariate regression method to the total sample and to the radio quiet and radio loud subsamples respectively. Table 3 summarizes our OLS bisector fitting results and lists the fitting parameters in equation (1) with errors in one-sigma confidence level and the dispersions (σ_r)[2]. The fitting result from Merloni et al. (2003) is also listed for comparison. Compared with the fundamental plane relation of Merloni et al. (2003), our results from the total sample of 115 sources and both the radio loud and radio quiet subsamples give a much smaller black hole mass dependence (ξ_{RM}). And much larger radio–X-ray correlation slopes ($\xi_{RX} > 1$) are found in the fittings of the total sample and the radio loud subsample when compared with the value of $\xi_{RX} = 0.60$ in Merloni et al. (2003). The radio–X-ray correlation slope ($\xi_{RX} = 0.85$) in the result of radio quiet subsample is also larger than that in Merloni et al. (2003).

The result of the Eddington luminosity scaled luminosity fitting for radio quiet sources is:

$$Log(\frac{L_r}{L_{Edd}}) = (0.86 \pm 0.10) Log(\frac{L_X}{L_{Edd}}) + (-5.08 \pm 0.19), \quad (6)$$

where errors are in one-sigma confidence level.

Fig. 5 plots the fitting relations for radio quiet sources (eq. (4) and (6)) plus all the data points (including radio-loud sources) in different radio loudness bins with the x coordinate represents the quantity calculated from these two equations for radio-quiet sources.

The first thing we find out with our data is that our fundamental relationships are not sensitive to the black hole mass no matter the sources are radio loud or radio quiet (see Table 3). The correlation slope value ξ_{RM} is nearly zero within uncertainties for all the three fittings, which is different from what was found by Merloni et al. (2003). This is not surprise

[2]We define the dispersion as the square root of the variance of the differences between the observed radio luminosity and that calculated from the fitting relation.

as our sample is uniform and includes only supermassive black holes whose masses are in a much narrower range compared to those in Merloni et al. (2003). In this case the black hole mass may not affect the relation significantly. In Fig. 6 we plot L_r/L_X ratio versus black hole mass (M) in logarithm, which shows that the dependence of radio to X-ray luminosity ratio on black hole mass is also very weak.

Secondly we get very different radio–X-ray correlations for the radio loud and radio quiet samples. The slope ξ_{RX} for our radio quiet sample is about 0.85 which is a little steeper than the result in Merloni et al. (2003), but still close to the value found in the hard state of GBHs (Gallo et al. 2003, $\xi_{RX} \sim 0.7$). For the total sample and the radio loud subsample, the parameter ξ_{RX} is around 1.33 and 1.39 respectively. Thus either a much different radiation mechanism or some additional effects must be taken into account for the radio loud sources.

In addition, we also obtain a tight relation between the Eddington luminosity scaled radio and X-ray luminosities for the radio quiet subsample with the correlation slope $\xi_{ERX} = 0.86$ and a dispersion $\sigma_r = 0.38$.

4. Discussions

Previous studies on the black hole fundamental plane relation mainly concerned about the relations of black hole mass, hard X-ray luminosity (eg. 2-10keV), and radio luminosity at or above 5GHz (Gallo et al. 2003; Merloni et al. 2003; Yuan & Cui 2005). In this work, we use the 0.1-2.4keV X-ray luminosity and 1.4GHz radio luminosity instead. If we assume that the X-ray and radio emission can be described as power laws with the typical spectral index in each band for all the sources, the corrections from hard to soft X-ray and from 5GHz to 1.4GHz should be linear and only change the constant item in the fundamental plan relation (Eq. (4)). However, the actual spectrum of individual sources in our sample is probably more complicated, especially in the soft X-ray band. The spectral parameters may change from one source to another according to different luminosity level or different dominated radiation mechanisms at different accretion rate. Thus any nonlinear relations between the hard/soft X-ray luminosities or 5GHz/1.4GHz radio luminosities for sources in our sample will change the correlation slopes and result in different correlations in our fittings from those obtained in previous works. On the other hand, the small differences in the radio and X-ray spectral index for radio-quiet and radio-loud subsamples (Yuan et al. 1998) may also lead to some differences in the derived black hole fundamental plane. Future detailed studies on the radio and X-ray spectral index for individual sources in our sample are expected to resolve this problem.

In this work we found very different black hole fundamental plane relations for radio loud and radio quiet broad line AGNs. Although whether such a difference is intrinsic or not deserves further studies, our results on the fundamental plane relation is probably helpful to investigate the underlying black hole accretion physics and may be used to constrain the theoretical models.

The fundamental plane relation with the X-ray emission dominated by the relativistic jet has been well discussed in literature. Heinz (2004) recently showed that the synchrotron emission from the scale invariant jet including the effect of radiation cooling can lead to a correlation of $L_R \propto M^0 L_X^{1.42}$ with typical scale invariant synchrotron jet parameters. Similar conclusions were also obtained from studies on Galactic black hole X-ray binaries (Yuan et al. 2005; Yuan & Cui 2005). Our derived fundamental plane correlation slope for radio loud sample seems consistent with this jet dominate X-ray model as well.

However, for radio loud AGNs the Doppler beaming effect from the relativistic jet should also be important. Doppler beaming can increase the jet intrinsic power by a factor of $\delta^{2+\alpha}$ (where δ is the beaming factor and α is the intrinsic power-law spectra index, i.e. $f_\nu \propto \nu^{-\alpha}$, Krolik (1999)) and may lead to a spurious observed correlation. There are two situations needed to be discussed when thinking about the beaming effect. One is that both the radio and X-ray fluxes are dominated by jet emission and they will be affected by the relativistic beaming to different levels according to the spectral index in different band. The other is that only the radio emission is from the jet and beamed while the X-ray emission is dominated by the accretion flow. Falcke et al. (2004) have studied the low-power accretion black hole systems where the radio and X-ray emissions are both jet dominated. They used a sample including both the stellar black hole systems and AGNs, and found that the scaling relation between radio and X-ray emissions is only slightly dependent on the beaming factors in the form of shifting along the fitted correlation line. However, such a jet dominated circumstance only exists in the low state of black hole systems (Gallo et al. 2003; Yuan & Cui 2005) and is thus possibly not the case for our sample. In our case for broad line AGNs, probably only the radio emission is beamed. Therefore, for AGNs with different radio-loudness this extra effect of relativistic beaming will cause parallel shifts from the intrinsic fundamental plane, and thus lead to a steeper correlation slope in the observed correlation.

We noticed that the beaming factor is hard to be measured directly for large sample of AGNs, so we use the radio loudness as a possible indicator of it. In Fig. 3 and Fig. 5 all radio loud sources are shown in a parallel distribution according to different radio loudness bins, which indicates the possibility that all of these sources may obey the same correlation as that of the radio quiet sources but it is shifted by a different level according to different radio loudness. If we take the radio quiet fundamental plane relation as an intrinsic one for

all AGNs with high accretion rate, the difference ($\delta LogL_r$ or $\delta Log(L_r/L_{Edd})$) between the observed radio luminosity and that derived from the radio quiet fundamental plane can be calculated. In Fig. 7 we plot $\delta LogL_r$ and $\delta Log(L_r/L_{Edd})$ versus radio loudness and tight correlations are found. As shown in this plot, the differences between the observed and estimated radio luminosity can be different in more than 3 orders of magnitude. This is not impossible for the extremely radio loud sources with a beaming factor greater than 10. Also the difference between the observed and calculated radio luminosities are tightly correlated with the radio loudness. Table 4 lists the partial Kendall's τ correlation coefficient between $\delta LogL_r$, $\delta Log(L_r/L_{Edd})$ and logarithm radio loudness when taking the logarithm observed radio luminosity as the third variable. The test shows that the correlation still exists when the effects of radio luminosity are excluded. Therefore we think that the observed fundamental plane for radio loud AGNs is unreliable unless the beaming effect can be removed.

When considering the fundamental plane for radio quiet sources only, the underlying physical mechanism is not very clear as well. We compared our results with the available accretion flow models discussed in Merloni et al. (2003) with corresponding parameters listed in Table 3 of their paper. As the ROSAT observations are in the soft X-ray band, we also investigated the model of multicolour thermal emission from the inner part of a standard thin disk (Shakura & Sunyaev 1973). Moreover, the jet dominated situation with radiation cooling effect is also considered. At last we found that our fitting result can be marginally matched when the magnetic field dependence on black hole mass and accretion rate in the form of $B^2 \propto M^{-1}\dot{m}$ and the X-ray luminosity has a non-linear dependence on accretion rate with a power-law index around 2. Such parameters can be satisfied in the radiatively inefficient accretion flow models (Narayan, Mahadevan & Quataert 1998). Similar conclusion was also found in Merloni et al. (2003). However, there is no evidence that the sources with radiatively inefficient accretion flow occupy a large percentage in our sample when considering the X-ray to Eddington luminosity ratio range (10^{-3} to 1, see the L_X/L_{Edd} histogram in Fig. 1). We noticed that the emission in soft X-ray band is complex and may come from different radiation mechanisms (Brunner et al. 1997) including the multicolor thermal emission from the inner part of an optically thick disk, inverse Compton emission, and free-free emission in the hot corona. So more analyses on the X-ray and radio spectra as well as accretion disk model studies are needed for obtaining more accurate physical explanations of such a fundamental plane relation.

5. Summary

With a uniform broad line AGN sample we have studied the fundamental plane relation in black hole accretion systems. Compared to previous works, we found that our fundamental plane relation has a much weaker dependence on the black hole mass. A very tight relation is also found between the Eddington luminosity scaled X-ray and radio luminosities for radio quiet sources. The non-linear dependence of radio luminosity on X-ray luminosity is different for radio loud and radio quiet AGNs. We attribute this to the relativistic jet in radio-loud AGNs. Especially the Doppler beaming effect from a relativistic jet can increase the intrinsic radio emission significantly and lead to a steeper slope of the fundamental plan relation. The derived fundamental plane relation for radio-quiet sources should better reflect the intrinsic physical correlations. However, the soft X-ray emission mechanisms of AGNs are complex and more reliable theoretical explanations are expected to be obtained only after further detailed spectral studies in soft X-ray and radio band on the individual AGNs in our sample can be done. Finally, we would like to mention that our black hole fundamental plane relation is derived from a flux-limited sample consisting of 115 broad line AGNs. Obviously more future studies with larger and better samples are needed to confirm our result.

We thank the anonymous referee for valuable suggestions and Fukun Liu, Lei Qian, Bingxiao Xu and Feng Yuan for helpful discussions. This work is supported by the NSFC funds (No. 10473001 & No. 10525313), the RFDP Grant (No. 20050001026) and the Key Grant Project of Chinese Ministry of Education (No. 305001).

REFERENCES

Akritas, M. G., & Siebert, J. 1996 MNRAS, 278, 919

Anderson, S. F., Voges, W., Margon, B. et al. 2003, AJ, 126, 2209

Becker, R. H., Helfand, D. J., White, R. L. et al. 2003, yCat., 8071, 0

Boroson, T. A., & Green, R. F. 1992, ApJS, 80, 109

Bregman, J. N. 2005, submitted to ApJ(astro-ph/0511368)

Brunner, H. et al. 1997, A&A, 326, 885

Falcke, H., Körding, E., & Markoff, S. 2004, A&A, 414, 895

Fender, R. P., Gallo, E., & Jonker, P. G. 2003, MNRAS, 343, L99

Gallo, E., Fender, R. P., & Pooley, G. G. 2003, MNRAS, 344,60

Heinz, S., & Sunyaev, R. A. 2003, MNRAS, 343, L59

Heinz, S., 2004, MNRAS, 355, 835

Isobe, T., Feigelson, E. D., Akritas, M. G., & Babu, G. J. 1990, ApJ, 364, 104

Kaspi, S., Smith, P. S., Netzer, H. et al. 2000, ApJ, 533, 631

Kaspi, S., Maoz, D., Netzer, H. et al. 2005, ApJ, 629, 61

Kellermann, K. I., Sramek, R., Schmidt, M. et al. 1989, AJ, 98, 1195

Krolik, J. H. 1999, Active galactic nuclei: from the central black hole to the galactic environment (Princeton: Princeton University press)

McLure, R. J., & Jarvis, M. J., 2002, MNRAS, 337, 109

Merloni, A., & Fabian, A. C. 2002, MNRAS, 332, 165

Merloni, A., Heinz, S., & Di Matteo, T. 2003, MNRAS, 345, 1057

Narayan, R., Mahadevan, R. Quataert, E., 1998, In Theory of Black Hole Accretion Disks, eds Abramowicz M., Bjornsson G., & Pringle J., Cambridge University Press

Narayan, R., & Yi, I. 1994, ApJ, 428, L13

Shakura, N. I., & Sunyaev, R. A. 1973, A&A, 24, 337

White, R. L., Becker, R. H., Helfand, D. J., Gregg, M. D. 1997, ApJ, 475, 479

Vestergaard, M., & Wilkes, B. J. 2001, ApJS, 134, 1

Wu, X-B., Wang, R., Kong, M. Z. et al. 2004, A&A, 424, 793

Yuan, F., Cui, W., & Narayan, R. 2005, ApJ, 620, 905

Yuan, F., & Cui, W. 2005, ApJ, 629, 408

Yuan, W., Brinkmann, W., Siebert, J., Voges, W. 1998, A&A, 330, 108

Table 1. The AGN sample

Name	z	Log($\frac{M}{M_\odot}$)	Log($\frac{L_X}{ergs^{-1}}$)	Log($\frac{L_r}{ergs^{-1}}$)	LogR
SDSS J000608.04-010700.8	0.949	8.770	45.456	41.272	1.433
SDSS J000710.01+005329.0	0.316	9.091	44.896	39.758	0.539
SDSS J000813.22-005753.3	0.139	8.305	43.817	39.268	1.082
SDSS J003847.96+003457.4	0.081	8.170	43.276	38.647	0.915
SDSS J004319.74+005115.3	0.308	9.301	44.561	39.779	0.647
SDSS J005441.19+000110.6	0.647	8.370	45.336	40.721	1.027
SDSS J005905.51+000651.5	0.719	8.979	45.387	43.777	3.821
SDSS J012100.73-001519.0	0.864	8.156	45.274	42.645	3.720
SDSS J012240.12-003239.7	0.883	8.966	45.360	40.469	0.283
SDSS J012528.83-000555.9	1.077	9.335	46.089	43.969	3.219
SDSS J012905.32-005450.6	0.707	8.527	44.987	41.427	1.795
SDSS J014644.82-004043.2	0.083	6.738	43.730	38.993	0.949
SDSS J015105.80-003426.3	0.335	8.803	44.688	40.273	1.614
SDSS J015950.24+002340.9	0.163	8.262	44.499	40.359	1.084
SDSS J020615.99-001729.1	0.043	8.123	43.504	38.392	0.142
SDSS J021225.57+010056.1	0.513	8.716	44.753	41.774	2.498
SDSS J022347.48-083655.5	0.261	7.828	44.198	39.435	0.824
SDSS J024240.31+005727.2	0.569	9.405	45.791	40.721	0.565
SDSS J073623.12+392617.8	0.118	8.126	44.683	39.241	0.371
SDSS J074242.18+374402.0	0.806	8.860	45.534	41.686	1.927
SDSS J075047.32+413033.5	1.184	8.605	45.779	41.223	0.551
SDSS J075407.95+431610.5	0.348	9.502	45.210	40.865	1.387
SDSS J075819.68+421935.1	0.211	8.305	44.797	39.475	0.360
SDSS J075838.14+414512.4	0.094	7.452	43.125	38.804	0.828
SDSS J080131.96+473616.0	0.157	8.883	44.830	40.751	1.585
SDSS J080322.48+433307.1	0.276	8.203	44.668	40.236	1.357
SDSS J083317.46+512422.3	0.591	8.055	45.155	40.049	0.497
SDSS J083525.17+482656.3	1.301	8.241	45.945	41.311	0.678
SDSS J084224.91+514501.1	0.797	8.813	45.231	40.665	0.615
SDSS J085442.00+575730.0	1.318	9.073	45.809	43.952	3.585
SDSS J085457.22+544820.5	0.256	7.499	44.219	39.517	0.847
SDSS J090145.28-000051.7	1.454	8.934	45.900	40.898	0.589
SDSS J090745.29+532421.5	0.711	9.529	45.367	41.299	1.399
SDSS J090910.08+012135.7	1.024	8.885	45.912	43.494	2.973
SDSS J090924.69+521632.6	0.410	9.443	44.720	41.752	2.371
SDSS J091205.16+543141.2	0.448	8.826	44.418	40.078	1.122
SDSS J091301.01+525928.9	1.377	9.236	46.199	41.558	0.347
SDSS J091333.65-004250.9	0.426	9.075	44.797	41.197	1.777
SDSS J091635.45+541426.9	0.284	8.069	44.228	40.572	2.115
SDSS J092856.27+013246.0	0.284	7.203	44.506	39.343	0.740
SDSS J092943.41+004127.3	0.587	8.799	45.508	40.459	0.456
SDSS J093200.08+553347.4	0.266	8.615	44.260	40.154	1.007
SDSS J093609.13-002639.7	0.141	7.114	43.691	38.689	0.467
SDSS J094042.92+021557.3	0.386	8.938	45.063	40.526	1.442
SDSS J100017.67+000523.7	0.905	8.410	45.715	42.620	3.013
SDSS J101044.51+004331.3	0.178	8.721	44.431	38.946	-0.171

Table 1—Continued

Name	z	Log($\frac{M}{M_\odot}$)	Log($\frac{L_X}{ergs^{-1}}$)	Log($\frac{L_r}{ergs^{-1}}$)	LogR
SDSS J101502.24+023128.1	0.218	7.905	43.858	40.231	1.812
SDSS J101527.26+625911.5	0.350	8.319	44.145	39.769	1.012
SDSS J101557.05+010913.6	0.780	9.286	45.802	42.596	2.037
SDSS J103214.52+635950.2	0.556	8.890	44.814	41.396	2.200
SDSS J105342.21-001420.1	0.676	8.840	44.962	41.987	2.875
SDSS J111221.82+003028.5	0.523	8.782	44.796	41.048	2.087
SDSS J111231.13-002534.2	0.544	8.477	45.363	41.251	2.097
SDSS J115024.79+015620.3	0.706	7.955	44.819	42.521	3.030
SDSS J115043.87-002354.0	1.976	9.683	46.441	44.808	3.775
SDSS J115542.53+021411.0	0.873	8.977	45.254	42.394	2.418
SDSS J120332.94+022934.6	0.077	7.453	43.987	38.549	0.265
SDSS J121347.52+000129.9	0.962	8.811	45.498	42.338	2.126
SDSS J123200.01-022404.7	1.043	9.004	45.524	43.895	3.235
SDSS J125337.35-004809.5	0.427	7.862	44.431	39.715	0.679
SDSS J125500.48+034043.0	0.437	8.578	44.980	41.759	2.483
SDSS J125519.69+014412.3	0.343	9.310	45.355	39.845	-0.019
SDSS J125945.18+031726.1	1.528	9.156	45.798	42.539	2.429
SDSS J130554.15+014929.8	0.733	9.430	45.300	42.062	2.189
SDSS J134113.93-005315.1	0.237	8.058	44.413	40.055	1.255
SDSS J134739.83+622149.5	0.804	8.582	45.214	40.810	1.650
SDSS J134948.39-010621.8	0.600	9.100	45.223	40.389	0.154
SDSS J135351.58+015153.8	1.608	8.862	45.833	43.666	3.300
SDSS J135425.23-001358.0	1.512	9.485	46.077	42.548	1.769
SDSS J135527.98+015527.4	1.732	8.654	45.905	42.294	1.874
SDSS J140104.87+004332.7	0.665	9.222	45.138	40.506	0.428
SDSS J140127.69+025606.1	0.265	7.692	44.083	39.881	1.525
SDSS J140710.59-004915.2	1.510	8.243	46.055	42.257	2.014
SDSS J141556.84+052029.5	0.126	8.031	43.920	38.790	0.423
SDSS J142339.88+043634.8	1.649	9.120	45.773	42.329	2.415
SDSS J142519.16+035425.8	0.792	8.302	45.072	41.768	2.520
SDSS J142545.90+002242.7	0.326	7.898	44.502	41.452	2.742
SDSS J143244.44-005915.1	1.027	9.335	45.618	41.958	1.554
SDSS J143641.94+022940.5	0.772	8.823	45.372	41.771	1.967
SDSS J145002.46+001629.3	0.957	9.087	45.577	41.813	2.075
SDSS J145126.16+032643.3	0.479	9.560	44.909	40.350	1.034
SDSS J150759.73+041512.2	1.701	9.496	47.432	43.486	2.363
SDSS J150935.97+574300.5	1.705	9.324	45.490	41.386	0.482
SDSS J150940.68+571811.8	0.817	8.832	45.136	42.074	2.325
SDSS J151441.13+555932.7	1.190	8.905	45.141	40.720	0.979
SDSS J154751.94+025550.8	0.098	7.940	43.981	38.892	0.644
SDSS J154929.44+023701.1	0.414	8.712	45.358	42.922	3.395
SDSS J155607.44+552436.2	0.434	8.052	44.079	40.083	0.736
SDSS J155620.24+521520.0	0.227	8.067	44.358	39.490	0.609
SDSS J160623.57+540555.8	0.876	8.754	45.067	42.807	2.615
SDSS J160713.91+483326.2	0.125	8.538	43.876	39.126	0.931
SDSS J160732.86+484619.9	0.146	7.868	43.225	39.052	0.640

Table 1—Continued

Name	z	Log($\frac{M}{M_{\odot}}$)	Log($\frac{L_X}{ergs^{-1}}$)	Log($\frac{L_r}{ergs^{-1}}$)	LogR
SDSS J160913.19+535429.5	0.992	9.143	45.085	42.348	2.186
SDSS J161156.31+521116.8	0.041	7.575	42.355	38.296	0.762
SDSS J163709.32+414030.8	0.760	9.329	44.918	41.300	1.040
SDSS J163856.53+433512.5	0.339	9.233	44.513	41.345	2.290
SDSS J164108.72+433612.3	1.068	9.487	45.192	41.801	1.715
SDSS J164224.30+444509.8	0.368	7.878	45.100	40.138	1.045
SDSS J164258.81+394836.9	0.593	9.060	45.730	44.026	3.334
SDSS J164829.25+410405.5	0.852	8.436	44.720	42.872	3.118
SDSS J165005.47+414032.4	0.585	8.906	45.174	42.461	2.929
SDSS J165641.51+372639.7	0.484	8.211	44.326	39.879	0.896
SDSS J165819.54+623823.1	0.703	8.603	44.910	40.667	1.069
SDSS J170306.09+615244.3	1.919	9.484	45.710	43.280	2.378
SDSS J171300.69+572530.2	0.360	8.250	44.397	39.821	0.698
SDSS J171936.70+604748.1	1.076	8.059	45.290	41.777	1.849
SDSS J172051.15+620944.3	1.010	9.065	45.473	41.831	1.919
SDSS J172206.03+565451.6	0.425	7.473	45.096	41.484	2.323
SDSS J172659.45+594017.8	0.725	9.085	44.742	41.834	2.626
SDSS J172750.70+575112.8	0.592	8.841	44.856	40.472	1.809
SDSS J220908.24-005558.9	0.530	8.748	45.261	41.423	2.269
SDSS J221542.29-003609.7	0.099	7.578	43.859	38.762	0.564
SDSS J231845.81-000754.8	0.866	8.545	45.461	41.285	1.885
SDSS J233624.04+000246.0	1.095	9.103	45.591	42.034	1.751
SDSS J235156.12-010913.3	0.174	9.093	45.079	41.686	2.404

Table 2. The partial correlation test for the fundamental plane correlation

X	Y	Z	Type	Number	τ	σ	P_{null}
logLx	logLr	logD	radio loud	76	0.305	0.0738	3.591E-05
logLx	logLr	logD	radio quiet	39	0.367	0.1059	5.295E-04
logLx	logLr	logD	total	115	0.279	0.0562	7.009E-07
logLx	logLr	logM	radio loud	76	0.502	0.0550	<1.000E-10
logLx	logLr	logM	radio quiet	39	0.623	0.0929	<1.000E-10
logLx	logLr	logM	total	115	0.491	0.0461	<1.000E-10
logM	logLr	logLx	radio loud	76	0.131	0.0653	4.475E-02
logM	logLr	logLx	radio quiet	39	0.179	0.0690	9.270E-03
logM	logLr	logLx	total	115	0.182	0.0492	2.224E-04
logM	logLx	logLr	radio loud	76	0.202	0.0691	3.473E-03
logM	logLx	logLr	radio quiet	39	0.297	0.0960	2.013E-03
logM	logLx	logLr	total	115	0.290	0.0531	4.608E-08
log(Lx/L_{Edd})	log(Lr/L_{Edd})	logD	radio loud	76	0.386	0.0633	1.099E-09
log(Lx/L_{Edd})	log(Lr/L_{Edd})	logD	radio quiet	39	0.526	0.1085	1.251E-06
log(Lx/L_{Edd})	log(Lr/L_{Edd})	logD	total	115	0.307	0.0482	2.028E-10
log(Lx/L_{Edd})	log(Lr/L_{Edd})	logM	radio loud	76	0.497	0.0515	<1.000E-10
log(Lx/L_{Edd})	log(Lr/L_{Edd})	logM	radio quiet	39	0.587	0.0777	<1.000E-10
log(Lx/L_{Edd})	log(Lr/L_{Edd})	logM	total	115	0.444	0.0434	<1.000E-10
logM	log(Lr/L_{Edd})	log(Lx/L_{Edd})	radio loud	76	0.143	0.0646	2.695E-02
logM	log(Lr/L_{Edd})	log(Lx/L_{Edd})	radio quiet	39	-0.038	0.0962	6.925E-01
logM	log(Lr/L_{Edd})	log(Lx/L_{Edd})	total	115	0.211	0.0518	4.554E-05
logM	log(Lx/L_{Edd})	log(Lr/L_{Edd})	radio loud	76	-0.269	0.0672	6.421E-05
logM	log(Lx/L_{Edd})	log(Lr/L_{Edd})	radio quiet	39	-0.049	0.0992	6.237E-01
logM	log(Lx/L_{Edd})	log(Lr/L_{Edd})	total	115	-0.217	0.0567	1.295E-04

Table 3. The derived fundamental plane relation

Subsample	Number	ξ_{RX}	ξ_{RM}	Const.	σ_r
Total	115	1.33 ± 0.15	0.30 ± 0.18	-0.40 ± 0.14	0.89
Radio loud	76	1.39 ± 0.17	0.17 ± 0.21	-0.17 ± 0.21	0.77
Radio quiet	39	0.85 ± 0.10	0.12 ± 0.13	-0.77 ± 0.07	0.38
Merloni et al. (2003)	-	0.60 ± 0.11	$0.78^{+0.11}_{-0.09}$	$7.33^{+4.05}_{-4.07}$	0.88

Table 4. The partial correlation test for the beaming effect

X	Y	Z	Type	Number	τ	σ	P_{null}
$\delta log L_r$	log r	$\log L_r$	radio loud	76	0.514	0.0794	<1.000E-10
$\delta log L_r$	log r	$\log L_r$	radio quiet	39	0.437	0.0778	1.924E-08
$\delta log L_r$	log r	$\log L_r$	total	115	0.590	0.0589	<1.000E-10
$\delta log \frac{L_r}{L_{Edd}}$	log r	$\log L_r$	radio loud	76	0.504	0.0938	7.676E-08
$\delta log \frac{L_r}{L_{Edd}}$	log r	$\log L_r$	radio quiet	39	0.369	0.0792	3.136E-06
$\delta log \frac{L_r}{L_{Edd}}$	log r	$\log L_r$	total	115	0.576	0.0616	<1.000E-10

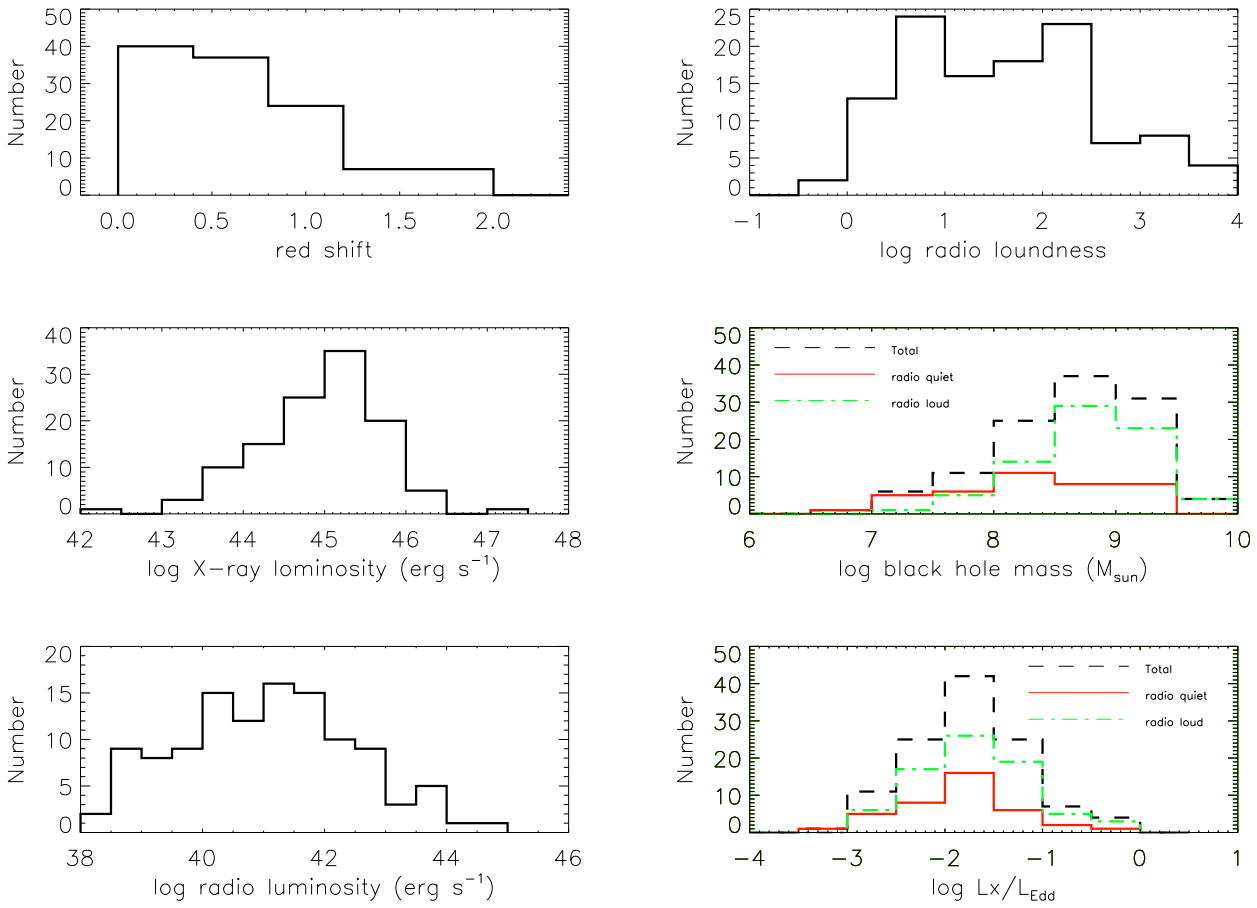

Fig. 1.— The global properties of the AGN sample with the upper panel show the histograms of redshift and logarithm radio loudnesses, middle panel the logarithm X-ray 0.1-2.4keV and black hole mass (in unit of $M_\odot$), and bottom panel the rest frame 1.4GHz radio luminosities and ratios of X-ray to Eddington luminosity ($L_{Edd} = 1.26 \times 10^{38}(M/M_\odot) erg\, s^{-1}$). For the mass and luminosity ratio histograms, the dashed lines give the distributions of the total sample while the solid and dash-dotted lines represent the radio quiet and radio loud subsample.

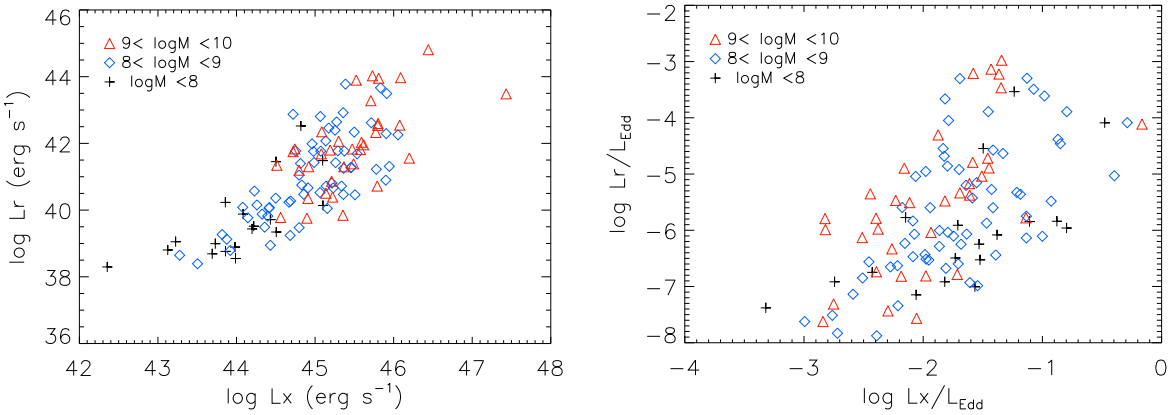

Fig. 2.— The 1.4GHz rest frame radio luminosity versus the 0.1-2.4keV X-ray luminosity with different symbols corresponding to different bins of logarithm black hole mass (in unit of $M_{\odot}$). In the left panel we plot the logarithm luminosities directly while in the right panel we scale the luminosity with the Eddington luminosity.

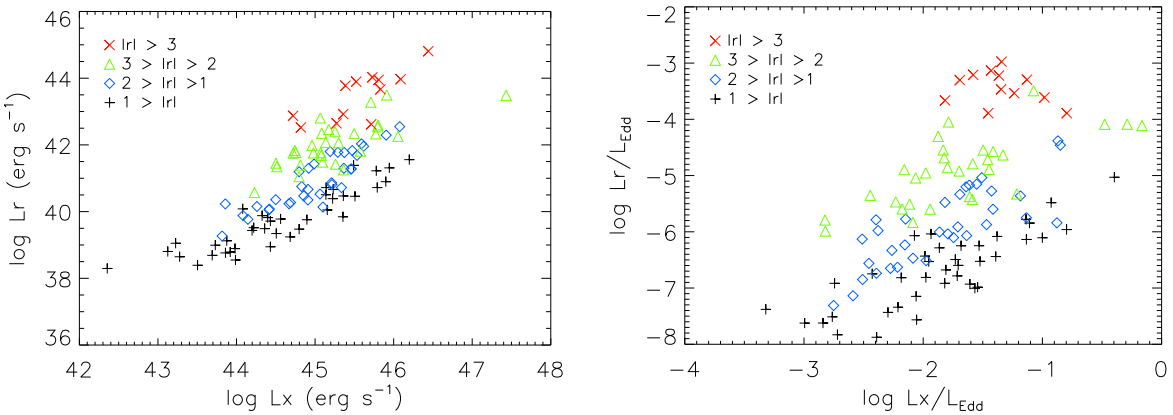

Fig. 3.— The rest frame 1.4GHz radio luminosity versus 0.1-2.4keV X-ray luminosity with different symbols represent different bins of logarithm radio loudness (lrl) . In the left panel we plot the logarithm luminosities directly while in the right panel we scale the luminosity with the Eddington luminosity.

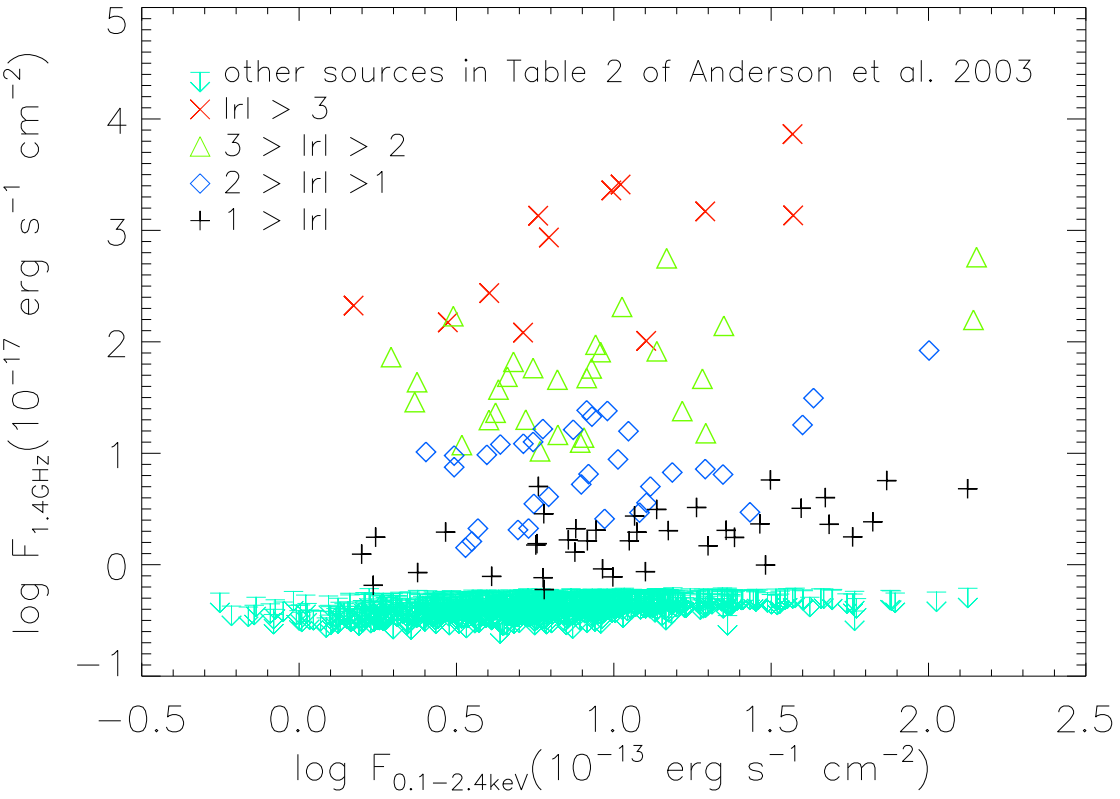

Fig. 4.— The rest frame 1.4GHz radio flux versus 0.1-2.4keV X-ray flux for the broad permitted line AGN sample in Table 2 of Anderson et al. (2003). For the 115 sources in our sample, different symbols represent those in different bins of logarithm radio loudness. For other sources without FIRST detection, we take 0.45mJy as an upper limit of the observed 1.4GHz radio flux (Becker et al. 2003).

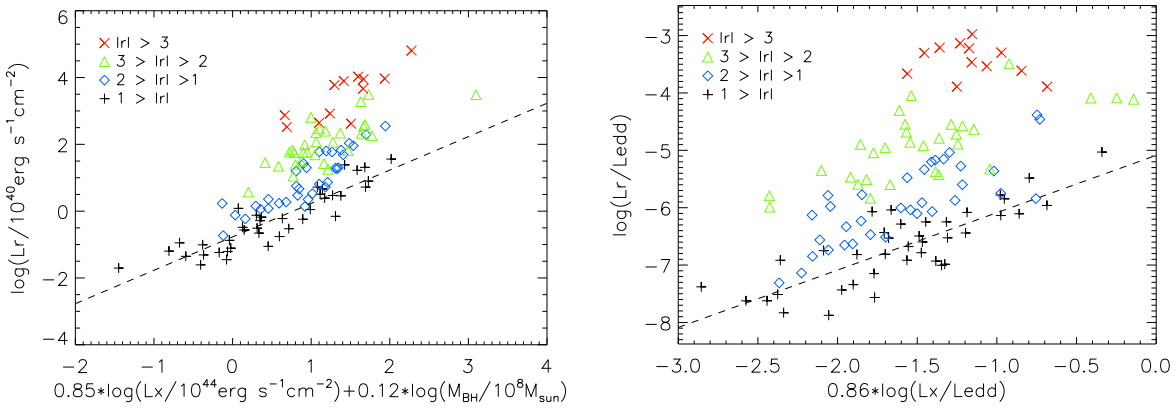

Fig. 5.— Fitting results. The left panel shows all the AGNs in the sample according to the radio quiet fundamental plane relation with different symbols corresponding to different logarithm radio loudness (lrl) bins. The right panel shows the Eddington luminosity scaled radio and X-ray luminosities according to the fitting result for radio quiet sources. The dashed line represents the best fitting relation with the radio quiet sources only.

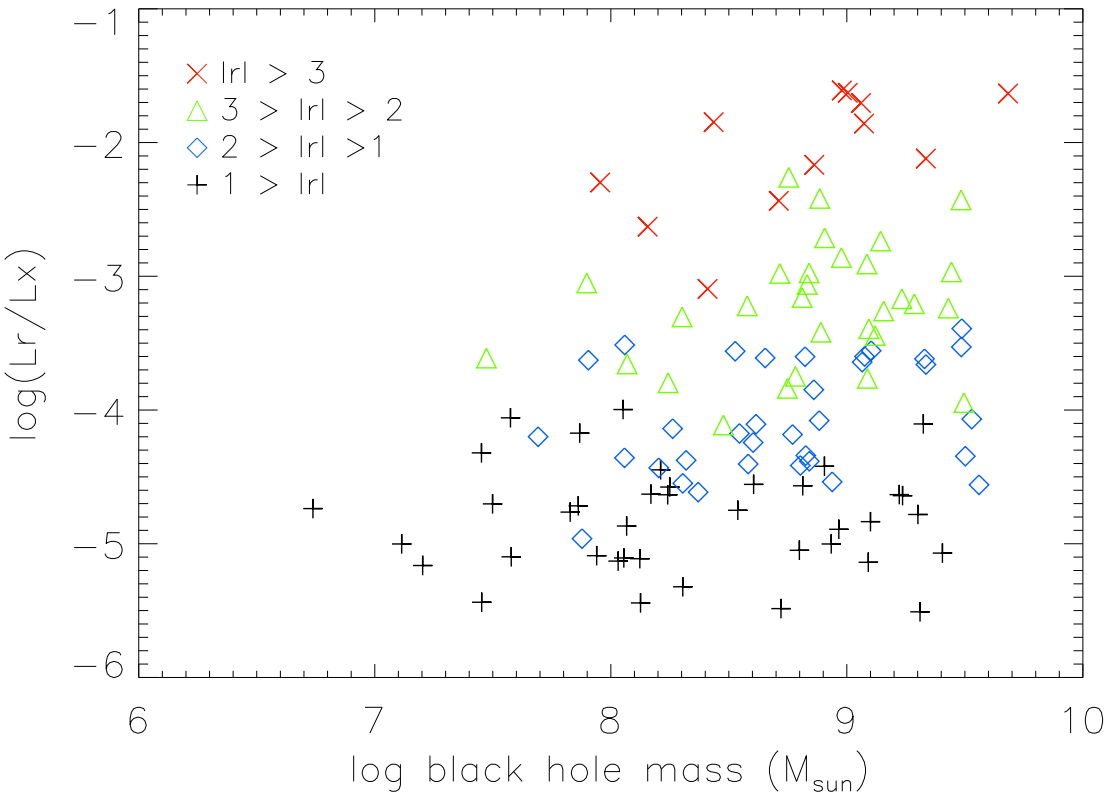

Fig. 6.— The ratios of radio and X-ray luminosity are ploted versus the black hole masses in logarithm. Different symbols represent sources in different bins of logarithm radio loudness.

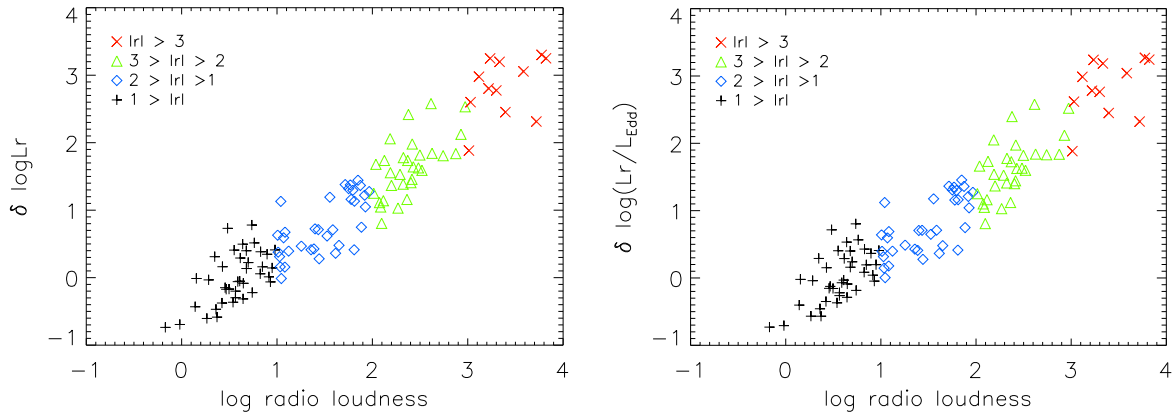

Fig. 7.— The differences ($\delta LogL_r$) between the observed radio luminosity and that derived from the fundamental plane of the radio quiet AGNs for all AGNs in the sample with different logarithm radio loudness (lrl) bins are ploted versus the logarithm radio loudness. The left panel gives the logarithm radio luminosity difference calculated with equation (4) using the fitting result from the radio quiet sources in Table 3, while the right panel gives the differences calculated with equation (6).